J|A|C|S ARTICLES

Published on Web 08/07/2009

Mechanistic Study of the sPLA$_2$-Mediated Hydrolysis of a Thio-ester Pro Anticancer Ether Lipid

Lars Linderoth,[‡,||] Peter Fristrup,[*,‡,§] Martin Hansen,[‡] Fredrik Melander,[⊥] Robert Madsen,[‡] Thomas L. Andresen,[¶] and Günther H. Peters[*,†]

Department of Chemistry, MEMPHYS-Center for Biomembrane Physics, Technical University of Denmark, DK-2800 Kgs. Lyngby Denmark, Department of Chemistry, Technical University of Denmark, DK-2800 Kgs. Lyngby, Denmark, Materials and Process Simulation Center (139-74), California Institute of Technology, Pasadena, California 91125, LiPlasome Pharma A/S, Technical University of Denmark, DK-2800 Kgs. Lyngby, Denmark, and DTU Nanotech, Technical University of Denmark, DK-4000 Roskilde, Denmark

Received February 23, 2009; E-mail: ghp@kemi.dtu.dk; pf@kemi.dtu.dk

Abstract: Secretory phospholipase A$_2$ (sPLA$_2$) is an interesting enzyme for triggered liposomal drug delivery to tumor tissue due the overexpression of sPLA$_2$ in cancerous tissue. A drug delivery system based on the triggered release of therapeutics from sPLA$_2$-sensitive liposomes constituted of pro anticancer ether lipids, which become cytotoxic upon sPLA$_2$-catalyzed hydrolysis has previously been established. To optimize the hydrolysis rate of the lipids and thereby optimizing the release profile of the drugs from the liposomes, we have synthesized a thio-ester pro anticancer ether lipid. Liposomes constituted of this lipid showed an altered rate of hydrolysis by sPLA$_2$. We have tested the cytotoxicity of the thio-ester pro anticancer ether lipids toward cancer cells, and the results showed that the cytotoxicity is indeed maintained upon sPLA$_2$ exposure. To further understand the origin for the observed different hydrolysis rates for the esters, we have applied molecular dynamics simulations and density functional theory. The combination of these theoretical methods has given valuable insight into the molecular mechanism for sPLA$_2$ action on sulfur-containing phospholipids. It appears that the enzyme-catalyzed hydrolysis of thio-esters follow a different pathway compared to the hydrolysis pathway of the free thio-ester.

1. Introduction

Secretory phospholipases A$_2$ (sPLA$_2$s) are small, water-soluble enzymes where 10 members of the sPLA$_2$ family are known so far.[1] These enzymes catalyze the hydrolysis of phospholipids in the *sn*-2 position, generating lysophospholipids and fatty acids.[2] Moreover, several characteristics are associated with this family of enzymes, for instance, the Ca^{2+} requirements for enzymatic activation, the low molecular weights (14 to 19 kDa) and their secretion from cells.[3] Although the sPLA$_2$ family shares many characteristics, it is intriguing that some of the group members show different substrate specificities. The sPLA$_2$-IIA subtype is mainly active toward negatively charged phospholipids, whereas the sPLA$_2$-V and -X subtypes hydrolyze both anionic and zwitterionic phospholipids.[1] sPLA$_2$-IIA has proven especially interesting for chemotherapeutic intervention as high levels of the enzyme have been reported in human colorectal adenomas and in neoplastic prostatic tissue.[3] We have exploited the occurrence of high levels of sPLA$_2$-IIA in tumor cells in a new drug delivery concept, where sPLA$_2$-sensitive liposomes with entrapped chemotherapeutics deliver their cargo specifically at the tumor site.[4] One of the challenges in drug delivery systems is to optimize the rate of hydrolysis of the lipids, thereby optimizing the release profile of the drugs from the liposomes.[5] We have therefore explored phospholipid analogues and could previously demonstrate that sPLA$_2$ is capable of hydrolyzing phospholipids with very diverse structures. Small substituents in the *sn*-1 position can be tolerated by the enzyme[6,7] and even shifting the phosphate headgroup from the *sn*-3 position to the C-2 position is tolerated by the enzyme.[8] To further elucidate the unique properties of this enzyme and to fine-tune the hydrolysis rate of phospholipid analogues, we have modified the glycerol backbone of phospholipids by replacing the conventional ester with a thio-ester. We have thus synthesized a thio-ester pro anticancer ether lipid (S-ProAEL), monitored the rate of hydrolysis catalyzed by

† MEMPHYS-Center for Biomembrane Physics, Technical University of Denmark.
‡ Department of Chemistry, Technical University of Denmark.
§ Materials and Process Simulation Center (139-74), California Institute of Technology.
⊥ LiPlasome Pharma A/S, Technical University of Denmark.
¶ DTU Nanotech, Technical University of Denmark.
|| Present address: Novo Nordisk A/S, Protein and Peptide Chemistry 3, Novo Nordisk Park, DK-2760 Måløv, Denmark.

(1) Murakami, M.; Kudo, I. *Biol. Pharm. Bull.* **2004**, *27*, 1158–1164.
(2) Six, D. A.; Dennis, E. A. *Biochim. Biophys. Acta, Mol. Cell. Biol. Lipids* **2000**, *1488*, 1–19.
(3) Laye, J. P.; Gill, J. H. *Drug Discovery Today* **2003**, *8*, 710–716.
(4) Andresen, T. L.; Jensen, S. S.; Madsen, R.; Jørgensen, K. *J. Med. Chem.* **2005**, *48*, 7305–7314.
(5) Andresen, T. L.; Jensen, S. S.; Jørgensen, K. *Prog. Lipid Res.* **2005**, *44*, 68–97.
(6) Linderoth, L.; Peters, G. H.; Jørgensen, K.; Madsen, R.; Andresen, T. L. *Chem. Phys. Lipids* **2007**, *146*, 54–66.
(7) Linderoth, L.; Andresen, T. L.; Jørgensen, K.; Madsen, R.; Peters, G. H. *Biophys. J.* **2008**, *94*, 14–26.
(8) Peters, G. H.; Møller, M. S.; Jørgensen, K.; Rönnholm, P.; Mikkelsen, M.; Andresen, T. L. *J. Am. Chem. Soc.* **2007**, *129*, 5451–5461.

 © 2009 American Chemical Society

Scheme 1[a]

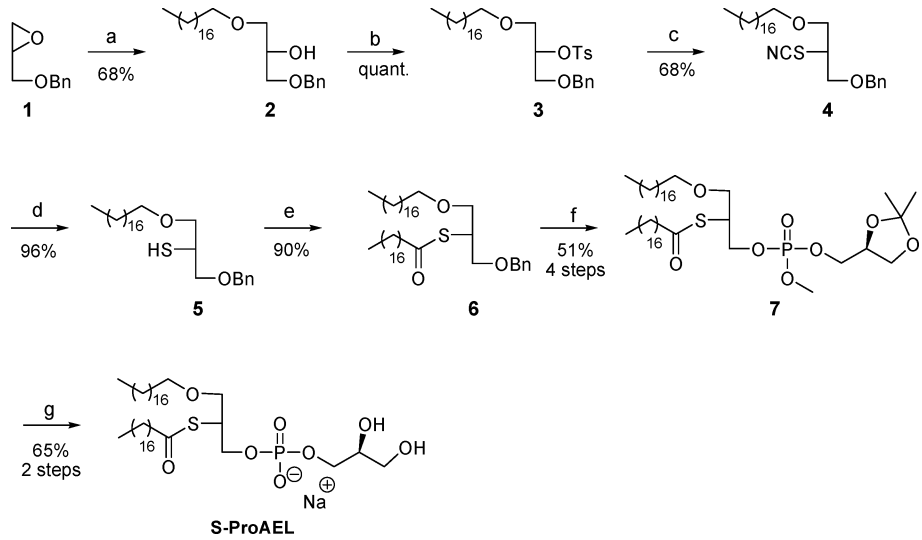

[a] Reagents and conditions: (a) NaH, octadecanol, THF/DMF; (b) TsCl, Et_3N, DMAP, DCM; (c) KSCN, DMF; (d) $LiAlH_4$, Et_2O; (e) octadecanoic acid, DCC, DMAP; (f) (i) BCl_3, DCM, −30 °C, (ii) $(i\text{-Pr})_2NP(OMe)Cl$, TMP, DCM, (iii) 5-Ph-1*H*-tetrazole, (*R*)-isopropylidene glycerol then *t*-BuOOH; (g) (i) Me_3N, DCM, CH_3CN, (ii) DCM, MeOH, HCl, (iii) $NaHCO_3$.

$sPLA_2$ compared to the natural substrate (1,2-distearyl-*sn*-glycero-3-phosphoglycerol, DSPG) and determined the cytotoxicity of liposomes constituted of these lipids toward cancer cells.

To elucidate the mechanism of the thio-ester hydrolysis, we have performed molecular dynamics (MD) simulations and applied density functional theory, which have provided valuable insight into the mechanism of $sPLA_2$-catalyzed hydrolysis. The MD simulations indicated that both the thio-ester and natural substrate fit perfectly into the binding pocket. The density functional theory (DFT) calculations revealed that the enzyme-catalyzed thio-ester hydrolysis follows a mechanism similar to that observed for the oxygen-containing substrate, but with significantly higher activation energy. It seems that $sPLA_2$ has been optimized to catalyze the hydrolysis of oxygen esters through evolution and does not function equally well for the nonnatural thio-ester.

2. Results and Discussion

2.1. Synthesis of the S-ProAEL. The S-ProAEL was synthesized (Scheme 1) from the commercially available benzyl glycidyl ether **1**, which was reacted with octadecanol in the presence of sodium hydride to afford the glycerol **2**. Glycerol **2** was treated with TsCl in the presence of Et_3N and DMAP giving the desired sulfonate **3** in quantitative yield, which was reacted with potassium thiocyanide to afford thiocyanate **4** in 68% yield. Thiocyanate **4** was reduced to thiol **5** in 96% yield with $LiAlH_4$ and coupled with octadecanoic acid in the presence of DCC and DMAP to thio-ester **6** in 90% yield. The benzyl protecting group of thio-ester **6** was removed followed by insertion of the phosphate headgroup by the phosphoramidite method.[9] Thus, thio-ester **6** was treated with BCl_3 at −30 °C,[10] and the crude compound was reacted with commercially available methyl-*N,N*-diisopropylchlorophosphoramidite in the presence of 2,2,6,6-tetramethylpiperidine giving the corresponding amidite, which was reacted directly with 2,3-*O*-isopropylidine-*sn*-glycerol in combination with 5-phenyl-1*H*-tetrazole.[11] By treatment with *tert*-butylhydroperoxide, the generated phosphite was oxidized to the corresponding phosphate **7** in 51% yield from thio-ester **6**. The phosphate **7** was deprotected by the treatment with trimethyl amine followed by exposure to acidic conditions (DCM/MeOH/HCl solution) giving the desired S-ProAEL in 65% yield from phosphate **7**.

2.2. DSC, $sPLA_2$ Activity Measurements toward S-ProAEL Liposomes and Cytotoxicity of S-ProAEL. S-ProAEL was hydrated in aqueous HEPES buffer resulting in the formation of multilamellar liposomes (MLVs). MLVs were used for differential scanning calorimetry (DSC) measurements to obtain thermodynamic properties of the phospholipid. The scan revealed a main phase transition at 51.4 °C as a single peak. Subsequently, the MLVs were extruded as described previously, and the resulting small unilamellar S-ProAEL liposomes were tested for hydrolysis by $sPLA_2$.[6,7] We used 90° light scattering as an indirect measurement of hydrolysis as it detects morphology changes of the system. After the addition of the enzyme, significant changes in the 90° light scattering was observed in the system, indicating that $sPLA_2$-catalyzed hydrolysis of S-ProAEL occurred, resulting in the formation of nonbilayer-forming lysophospholipids and fatty acids and consequently in the breakdown of the liposomes (data not shown). These observations were further quantified using HPLC. Hence, at different time intervals after the addition of $sPLA_2$, samples were taken out, the reaction was quenched, and the samples were analyzed by HPLC. Similar experiments were carried out on small unilamellar vesicles composed of the naturally occurring phospholipid DSPG. The results are illustrated in Figure 1, which reveal that S-ProAEL is hydrolyzed more slowly than both the natural DSPG phospholipid and the conventional ProAEL (1-O-DSPG) by $sPLA_2$. As $sPLA_2$ is highly sensitive to the membrane interface and the membrane will reorganize at a certain hydrolysis threshold into, first, coexistence of liposomes and micelles and, consequently, into micelles and

(9) Beaucage, S. L.; Iyer, R. P. *Tetrahedron* **1993**, *49*, 10441–10488.
(10) Xia, J.; Hui, Y. Z. *Tetrahedron: Asymmetry* **1997**, *8*, 3019–3021.
(11) Andresen, T. L.; Skytte, D. M.; Madsen, R. *Org. Biomol. Chem.* **2004**, *2*, 2951–2957.

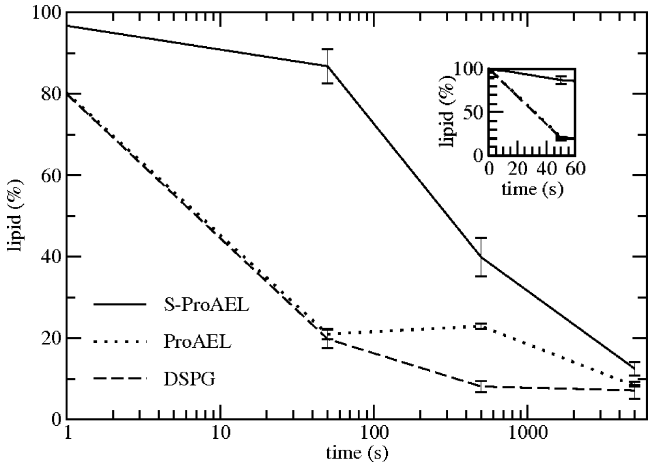

Figure 1. $sPLA_2$-catalyzed hydrolysis of liposomes composed of S-ProAEL (solid line), ProAEL (dotted line), or DSPG (dashed line) monitored by HPLC. The graph shows the amount of lipid (%) in the samples before the addition of the enzyme (0 s) and 50, 500, and 5000 s after the addition of $sPLA_2$. The inset shows initial decrease in lipid %. The average value and standard deviations are based on at least three independent experiments.

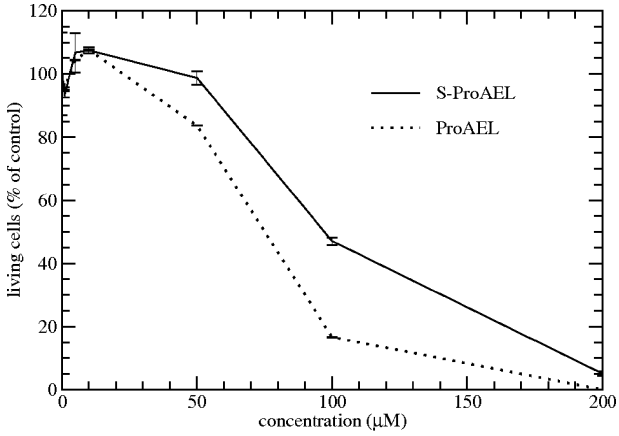

Figure 2. Cytotoxicity of S-ProAEL liposomes toward human colon carcinoma COLO205 cells that secrete $sPLA_2$-IIa. Cells were treated with the indicated concentrations of S-ProAEL liposomes (solid line) or ProAEL (dotted line) liposomes for 24 h. After washing, the cells were incubated for an additional 48 h in complete medium, and living cells were analyzed by an MTT assay. The average value and standard deviations are based on at least three independent experiments.

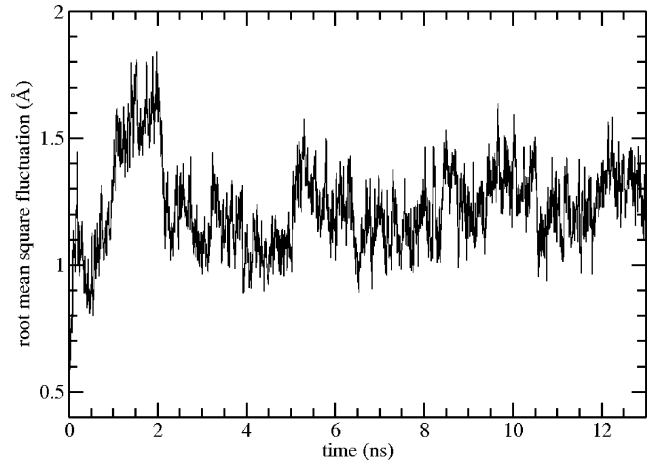

Figure 3. Time evolution of the root-mean-square fluctuation (rmsf) of Cα atoms of $sPLA_2$ with respect to the minimized structure. The rmsf data were extracted from an $sPLA_2$−S-ProAEL simulation, and the time evolution is representative for all simulations.

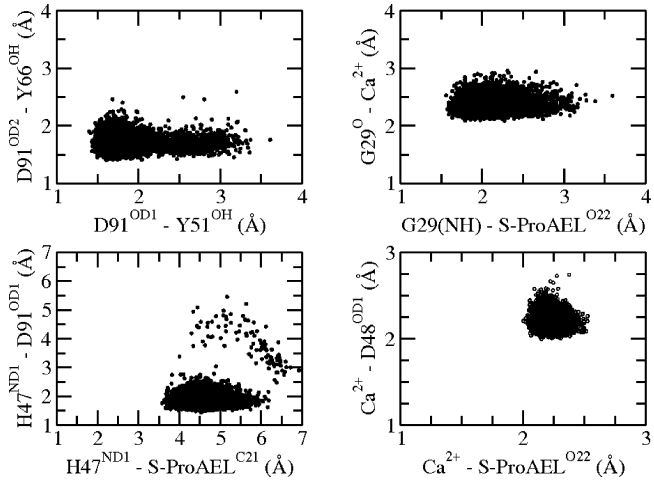

Figure 4. 2D scatter plots of distances between selected atoms that were chosen according to their importance in the calcium-dependent enzymatic reaction.[22] The distances were extracted from an $sPLA_2$−S-ProAEL simulation and are representative for all simulations. Atom types refer to the Protein Data Bank nomenclature. See the caption of Figure 5 for identification of the distances in the binding pocket.

possibly larger aggregated structures, it is only the initial rate of enzyme hydrolysis that can be compared.

The reduced hydrolysis rate measured for S-ProAEL is somewhat surprising, since thio-esters are often considered more labile than normal esters.[12,13] However, studies on 1-palmitoyl-2-thiopalmitoyl phosphatidylcholine (2-thioPC) phospholipids have also shown that these lipids are hydrolyzed more slowly than the natural phospholipids.[14] Studies on similar systems have shown that the chemical hydrolysis is the rate-limiting step in the interfacial catalysis by $sPLA_2$.[15] Hence, it appears that the slower hydrolysis of the S-ProAEL compared to the natural substrate is related either to less efficient binding of the thio-ester in the active site or that a different mechanism of hydrolysis is operating.

Before addressing this point, we have accessed the cytotoxicity of the S-ProAEL. It is known that ProAELs become toxic to various cancer cell lines upon hydrolysis by $sPLA_2$ due to the generation of AELs and fatty acids.[16] To ensure that the change from a natural ester to a thio-ester does not effect the prodrug properties of the S-ProAEL, we monitored whether the S-ProAELs become cytotoxic to human colon carcinoma COLO205 cells upon exposure to $sPLA_2$. The results of growth inhibition caused by the release of S-AELs are given in Figure 2.

When 50−200 μM of S-ProAEL liposomes were added to the cells, a pronounced growth inhibition was observed (the growth inhibition of the conventional ProAEL (1-O-DSPG) is shown as a reference). The results clearly demonstrate that the

(12) Sung, D. D.; Koo, I. S.; Yang, K.; Lee, I. *Chem. Phys. Lett.* **2006**, *432*, 426–430.
(13) Castro, E. A. *Chem. Rev.* **1999**, *99*, 3505–3524.
(14) Balet, C.; Clingman, K. A.; Hajdu, J. *Biochem. Biophys. Res. Commun.* **1988**, *150*, 561–567.
(15) Jain, M. K.; Yu, B. Z.; Rogers, J.; Gelb, M. H.; Tsai, M. D.; Hendrickson, E. K.; Hendrickson, H. S. *Biochemistry* **1992**, *31*, 7841–7847.
(16) Jensen, S. S.; Andresen, T. L.; Davidsen, J.; Høyrup, P.; Shnyder, S. D.; Bibby, M. C.; Gill, J. H.; Jørgensen, K. *Mol. Cancer Ther.* **2004**, *3*, 1451–1458.

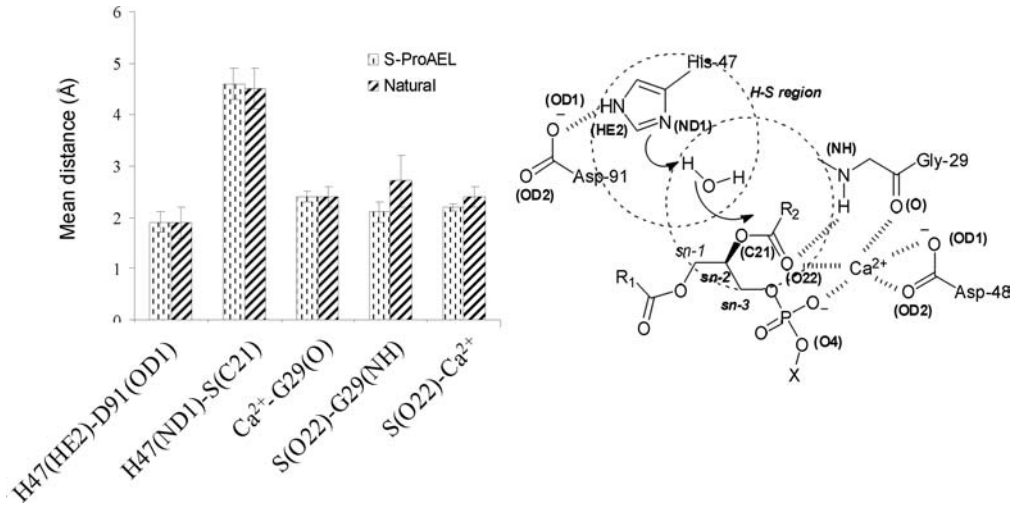

Figure 5. Mean distances of H47(HE2)−D91 (OD1), H47(ND1)−S(C21), Ca^{2+}−G29(O), S(O22)−G29(NH) and S(O22)−Ca^{2+} extracted from the simulations of the S-ProAEL-sPLA$_2$ complex and native substrate (left). Distances are averages over time and simulations. Schematic representations of the catalytic mechanism of sPLA$_2$ and part of the hydrogen-bonding network are shown to the right. Atom types given in parentheses refer to Protein Data Bank nomenclature. The overlap of the two circles indicates the *H*−*S* region.

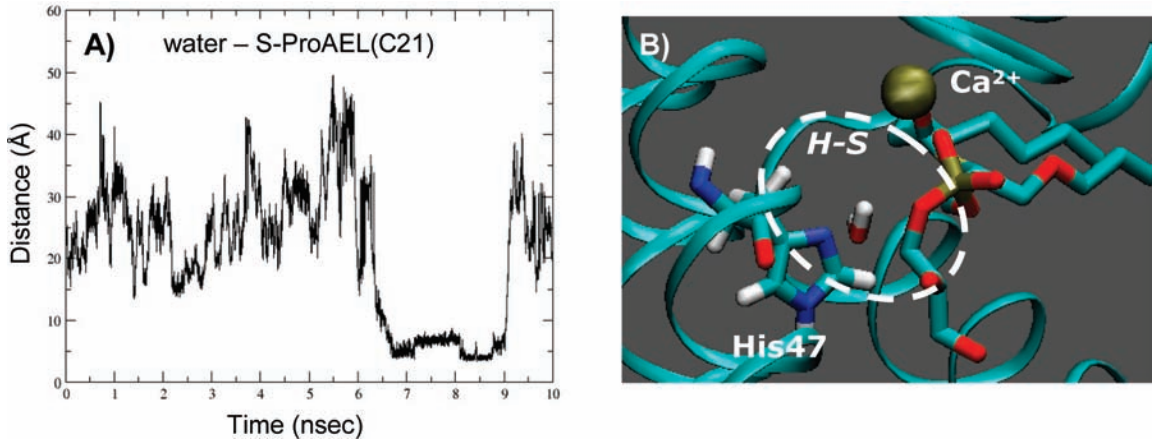

Figure 6. (A) Movement of a water molecule traveling into the active site of sPLA$_2$ as indicated by the distance between water and S-ProAEL(C21). (B) Snapshots of the active site of sPLA$_2$. The image is taken from a simulation of sPLA2−S-ProAEL complex. The secondary protein structure is shown in the ribbon mode and is colored green. His47, the substrate and a water molecule are shown in the liquorice mode and are colored according to the atom type (*H* = white, *N* = blue, *O* = red, *P* = gold). Ca^{2+} essential for sPLA$_2$ activity is shown in van der Waals mode and is colored gold. The circle indicates the *H*−*S* region, where the nucleophilic water molecule is positioned correctly such that hydrolysis can occur.

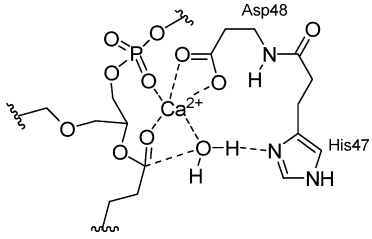

Figure 7. Illustration of the model system used in the DFT studies. The system consists of the crucial residues in the active site of sPLA$_2$, His47 and Asp48, together with the important cofactor calcium ion.

S-ProAEL liposomes are able to arrest the growth of COLO205 cells. Hence, the change from a hydroxyl group to a thiol in the *sn*-2 position of the AEL compounds does not significantly affect the cytotoxic properties of the phospholipid analogues.

2.3. Molecular Dynamics Simulations. To gain further insight into the origin that results in the different hydrolysis rates for the esters, we carried out molecular dynamics (MD) simulations and density functional theory calculations. The latter study focused on the energetics of the formation of the transition state, whereas MD simulations were carried out in order to study the binding mode of S-ProAEL with focus on substrate−sPLA$_2$ interactions and water accessibility to the active site cavity. We have previously demonstrated that even though some phospholipid analogues fit perfectly into the sPLA$_2$ binding pocket, these analogues can interfere with an incoming water molecule that participates in the hydrolysis.[7,8] Thus, the hydrolysis rate is reduced for these phospholipid analogues which in part could explain the experimentally observed reduced sPLA$_2$ activity profile toward these analogues.[7,8] We therefore first considered the Michaelis−Menten complex[17−21] and focused on the dynamics of the sPLA$_2$−substrate complex. MD simulations on the enzyme−substrate complexes were performed for at least 10 ns and repeated at least five times, starting from different initial configurations. The stability of the simulations was checked by monitoring the time evolution of the root-mean-square fluctuation (rmsf) of the Cα atoms of sPLA$_2$, and a representative graph is displayed in Figure 3. The rmsf reached a plateau within 2.5 ns, which was also observed for the other

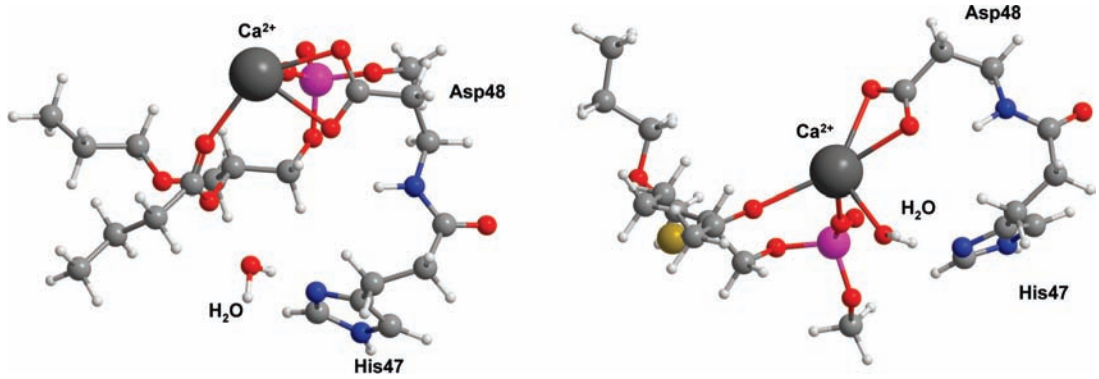

Figure 8. Conformations of the two fully minimized ester substrates are significantly different. Left: O-ester with the associated water molecule close to the carbonyl group. Right: The S-ester prefers a different location in the active site with a large distance between the water molecule and the carbonyl group. Color coding is as follows: Ca^{2+}: dark gray, P = pink, O = red, N = blue, S = yellow, C = light gray and H = white.

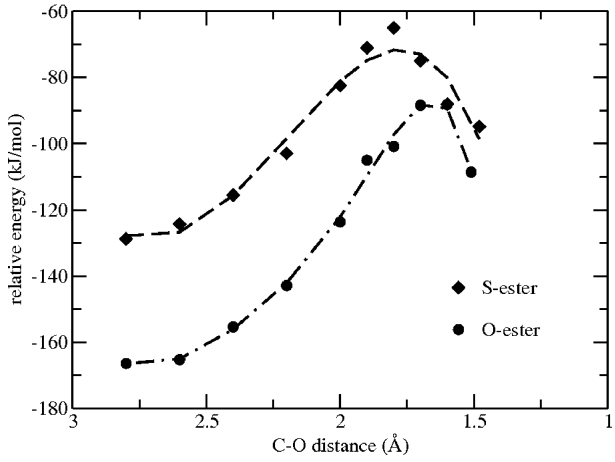

Figure 9. Energies for the two ester substrates calculated with different, fixed distances between the oxygen atom of the water molecule and the carbonyl carbon of the respective O-ester and S-ester.

simulations. We have therefore disregarded this time period in the calculation of the averaged rmsf and distances reported below.

The rmsf of the Cα atoms of the amino acids compared to the minimized protein structure averaged over time and trajectories was 1.2 ± 0.1 Å for the $sPLA_2$−S-ProAEL complex, which is comparable to 1.3 ± 0.1 Å for the $sPLA_2$−natural substrate complex.[8] This suggests that the S-ProAEL does not significantly affect the overall $sPLA_2$ structure, and we therefore focused on the binding pocket region. One of the requirements for catalysis is that a stable enzyme−substrate complex is formed and that several key distances between the enzyme and the substrate in the binding pocket are maintained.[22] In the following, we focused on the key distances involving the cofactor calcium, the substrate (S being S-ProAEL or natural substrate) Asp91 and His47: H47(HE2)−D91(OD1), H47(ND1)−S(C21), Ca^{2+}−G29 (O), Ca^{2+}−S(O22), Ca^{2+}−D48(OD1), Ca^{2+}−D48(OD2), S(O22)−G29(NH), D91(OD1)−Y51(OH) and D91(OD2)−Y66(OH). Atom types indicated in parentheses refer to the Protein Data Bank nomenclature, which will be used throughout. The distances were stable throughout the simulations, and in particular the distances between cofactor Ca^{2+} and S(O22) and D48 show only relatively small fluctuations, as indicated in the 2D scatter plots of distances between selected atoms in Figure 4. H47(HE2)−D91(OD1) shows relatively large fluctuations, which is also observed for D91(OD1)−Y51(OH). This is not surprising, since these residues are connected via a hydrogen-bonding network (Figure 5).

The time-averaged distances extracted from the simulations are presented in Figure 5 together with the data on the natural substrate. Numerical values are summarized in Table S1 (Supporting Information). A schematic representation of the binding pocket showing the key interactions used in the calculations is also illustrated in Figure 5.

The distances extracted from the S-ProAEL simulations are comparable to those from the $sPLA_2$-natural substrate simulations indicating that both substrates fit perfectly into the $sPLA_2$ binding pocket. This would suggest similar $sPLA_2$ activity toward both esters. However, this is in contradiction with our experimental observation that shows $sPLA_2$ activity toward the esters follows: natural substrate (DSPG) ≈ ProAEL > S-ProAEL (Figure 1). We therefore directed our attention to the accessibility of water molecules to the catalytic site cavity and monitored the movement of water molecules into the binding pocket in close proximity to His47(ND1) and the substrate S(C21) (hereafter referred to *H*−*S* region; Figure 5). An example of the trajectory of a water molecule extracted from an $sPLA_2$−S-ProAEL simulation is shown in Figure 6A. Initially, the water molecule diffuses randomly through the water phase (due to thermal motion) and is approximately 20−40 Å away from the *H*−*S* region. After ∼6.5 ns, the water molecule reaches the *H*−*S* region, where it is positioned for ∼2 ns before leaving the binding pocket again. A snapshot of the binding pocket of the $sPLA_2$−S-ProAEL complex is shown in Figure 6B. Here, the thio-ester analogue is perfectly positioned in the binding pocket to allow a water molecule to enter the *H*−*S* region, leading to a perfect alignment of the water molecule such that hydrolysis of the lipid can occur.

We further analyzed the simulations and monitored the frequency that a water molecule enters the *H*−*S* region. The probability of finding a water molecule in the *H*−*S* region is within the statistical uncertainties similar for the two esters. We find for S-ProAEL and the natural substrate that at a distance of 3.5 Å (4.5 Å) from His47(ND1) and the substrate S(C21), the relative water count is respectively 0.04 ± 0.05 (0.2 ± 0.3) and 0.1 ± 0.1 (0.4 ± 0.2). Clearly, the results from the MD simulations cannot explain why the hydrolysis of the thio-ester analogue is slower than that of the natural substrate.

We therefore decided to study the formation of the transition state for these two substrates, since earlier work has shown that the hydrolysis of free thio-esters does not necessarily follow the same mechanism as that of free oxygen-esters,[23] which is

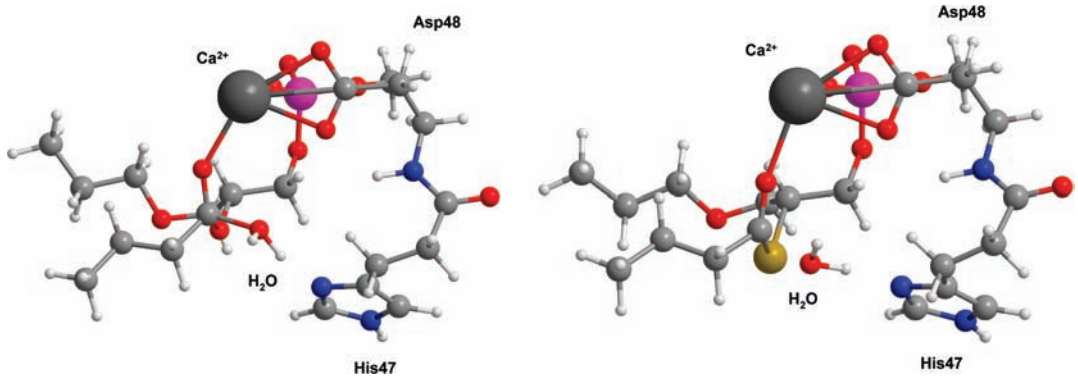

Figure 10. Examples of intermediate structures, which were optimized having a fixed distance between the carbonyl carbon atom of the respective esters and the oxygen atom in the water molecule. Left: O-ester, where the distance is fixed to 1.7 Å. Right: S-ester with the distance fixed to 1.8 Å (the bonds are automatically inserted by the visualization software and have no influence on the calculated energies). See caption of Figure 8 for the atom color code.

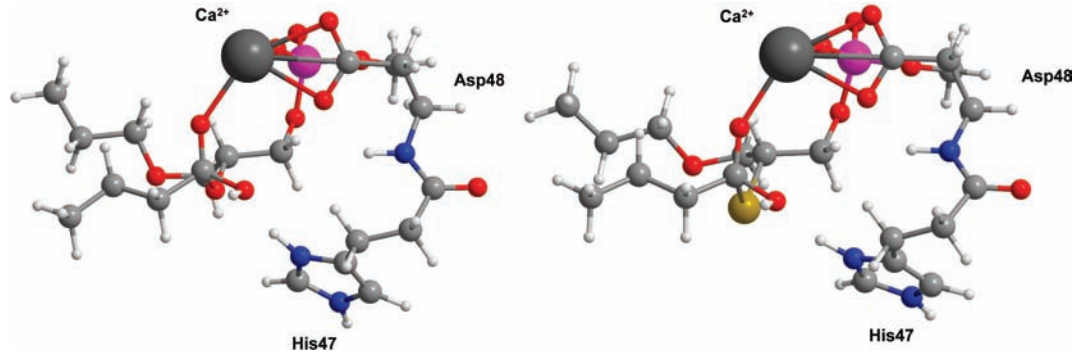

Figure 11. Structures of the tetrahedral intermediate obtained with the O-ester (left) and the S-ester (right). See caption of Figure 8 for the atom color code.

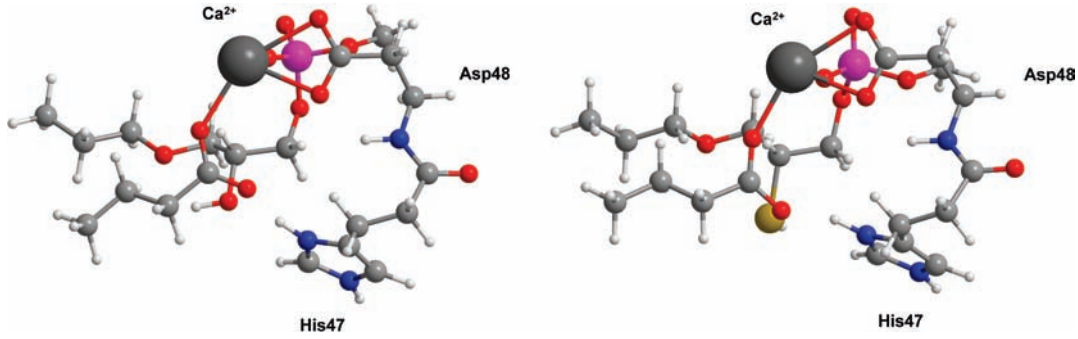

Figure 12. Fully minimized structures after proton-shift (left: O-ester; right: S-ester). In both cases, the alcohol/thiol and acid parts of the esters are clearly separated. See caption of Figure 8 for the atom color code.

generally considered to take place through formation of a tetrahedral intermediate.[24] Depending on the exact substitution pattern, the mechanism for the hydrolysis of thio-esters can instead proceed via an elimination−addition pathway.[23] To gain further insight into the exact mechanism involved in the enzymatic hydrolysis mediated by $sPLA_2$ and to rationalize the unexpected, less facile hydrolysis of the thio-containing ester compared to the natural substrate, we have performed DFT calculations. Since the rate-limiting step in the enzymatic reaction is the formation of the tetrahedral intermediate,[15] we were mainly interested in estimating the energy barrier of the formation of the tetrahedral intermediate for the two substrates as discussed in the next section. For simplicity, we refer to the natural substrate and the thio-ester respectively as O-ester and S-ester.

2.4. DFT Calculations. This methodology allows one to study the energetics and mechanism of enzymatic reactions,[25−29] and

(17) Peters, G. H.; Dahmen-Levison, U.; de Meijere, K.; Brezesinski, G.; Toxvaerd, S.; Möhwald, H.; Svendsen, A.; Kinnunen, P. K. J. *Langmuir* **2000**, *16*, 2779–2788.
(18) Peters, G. H. *Colloids Surf., B* **2002**, *26*, 84–101.
(19) Peters, G. H. Computer Simulations: A Tool for Investigating the Function of Complex Biological Macromolecules. In *Enzyme Functionality*; Svendsen, A., Ed.; Marcel Dekker, Inc.: New York, 2004; pp 97−148.
(20) Lambeau, G.; Gelb, M. H. *Annu. Rev. Biochem.* **2008**, *77*, 495–520.
(21) Leidy, C.; Linderoth, L.; Andresen, T. L.; Mouritsen, O. G.; Jørgensen, K.; Peters, G. H. *Biophys. J.* **2006**, *90*, 3165–3175.
(22) Scott, D. L.; White, S. P.; Otwinowski, Z.; Yuan, W.; Gelb, M. H.; Sigler, P. B. *Science* **1990**, *250*, 1541–1546.
(23) Douglas, K. T. *Acc. Chem. Res.* **1986**, *19*, 186–192.
(24) Bender, M. L. *Chem. Rev.* **1960**, *60*, 53–113.

recently, it has been shown that a selection of only a few key residues or even truncated residues often can provide a satisfying model for the real active site.[30−32] In line with this approach, the current study was carried out using a model system, where the enzyme part consisted of the two most crucial residues (His47 and Asp48) along with the required calcium ion. The histidine is believed to deprotonate the attacking water molecule, whereas the aspartate is responsible for binding the calcium ion. To limit the computational demand, the phospholipid headgroup was modeled by a simple methoxy group, and the fatty acid chains were both truncated to propyl. The system illustrated in Figure 7 consist of 71 atoms (including Ca^{2+}), which allowed treatment of the entire system with density functional theory (B3LYP[33−35] /LACVP[36]) including a SCRF-PCM[37,38] solvation model for water as described in the Supporting Information.

To identify the inherent conformational preferences for the two esters, initial conformational searches were carried out using the OPLS-2005 force-field. The lowest energy conformations of the two esters were virtually identical, except for the longer C−S bond (1.8 Å vs 1.6 Å for C−O), as expected. Since the MD calculations (*vide infra*) revealed that both substrates fit perfectly into the binding pocket and do not impair the incoming, nucleophilic water molecule, the differences in rate of hydrolysis must instead be a more direct result of the substitution of oxygen by sulfur. One example of the importance of this electronic difference was obtained when the anionic tetrahedral intermediates were optimized using DFT using an implicit solvation model for water. Here, it was only possible to obtain a stable energy minimum for the free O-ester, whereas the free S-ester spontaneously dissociated upon energy minimization. This is a strong indication that there is a difference in the inherit hydrolysis mechanism that each of the two esters follows under normal, basic aqueous conditions.

2.5. DFT Study Using a Model Active Site. As a reference state, we have chosen the empty active site, the isolated substrate, and an isolated water molecule. For both substrates the binding of the substrate in the binding pocket (along with the water molecule) is exothermic (∼−120−125 kJ/mol) when using the SCRF-PCM solvation model for water.[37,38] However, the two substrates adopt significantly different conformations (Figure 8), which result in a much longer distance between the carbonyl and the water molecule in the S-ester compared to the O-ester (S-ester: C−O 4.8 Å vs O-ester: 3.4 Å).

To determine the barrier for the deprotonation of the water molecule by histidine and subsequent addition to the carbonyl group, a series of energy minimizations were carried out. In each calculation, the distance between the carbon atom in the carbonyl and the oxygen in the water molecule was kept fixed to either 1.5, 1.6, 1.7, 1.8, 1.9, 2.0, 2.2, 2.4, 2.6, or 2.8 Å. For the shortest distance, the constraint was removed, and for both substrates, a stable tetrahedral intermediate was obtained. This illustrates that the model of the active site is capable of stabilizing this intermediate for the thio-ester (which was unstable in the absence of the model enzyme), thereby inducing an associative hydrolysis pathway for this substrate. When imposing a distance constraint of 2.8 Å, the relative energies for the two substrates become markedly different with the O-ester being more than 30 kJ/mol lower in energy as indicated in Figure 9, which displays the energy profile as the oxygen atom in the water molecule approaches the carbon atom in the carbonyl group of the ester.

The size and flexibility of the investigated systems prevent a stringent location of the transition state; however, as judged from the energy profiles, it is around 1.6−1.7 Å for the O-ester, and at a slightly longer distance for the S-ester at approximately 1.8 Å. In Figure 10, examples of the high-energy structures are shown.

The water molecule is situated in an intermediate position with the oxygen atom interacting with the carbonyl carbon of the respective esters, while one of the hydrogen atoms is hydrogen-bonded to the histidine. The calculated structures suggest that the crucial nucleophilic addition involves a simultaneous deprotonation of the water molecule by the histidine.[22] For both substrates, the tetrahedral intermediate is a stable energy minimum (Figure 11), and at this point in the reaction pathway, the difference in energy is 14 kJ/mol.

For both substrates, the tetrahedral intermediate has a higher energy than the initial complex of the reaction partners (O-ester: +48 kJ/mol, S-ester: +65 kJ/mol). We also inspected the elimination−addition pathway for both substrates by performing a series of calculations with fixed, increased C−O/S distances starting from the initial esters. As expected, this is very unfavorable for the O-ester, but also for the S-ester, this pathway cannot compete with the enzyme-assisted formation of the tetrahedral intermediate (see Supporting Information).

After formation of the tetrahedral intermediate, a proton shift to the ether-oxygen atom of the alcohol part of the ester should occur. The fidelity of this step was tested by manually moving the proton from the hydroxyl to the ether oxygen in the tetrahedral intermediate. Upon optimization, both substrates spontaneously separated to the acid and alcohol/thiol, as expected (Figure 12).

When comparing the fully energy minimized structures, the overall reaction was found to be 12 kJ/mol more favorable for the O-ester compared to the S-ester (−40 and −28 kJ/mol, respectively). The energy minimized structures again reveal differences between the O-ester and the S-ester, namely in the distance between the carbonyl group and the oxygen atom in the leaving alcohol. As observed earlier for the coordination of the water molecule, this distance is significantly longer for the S-ester (4.30 Å) than for the O-ester (3.32 Å), which again underlines that there are subtle but not negligible differences between the properties of these two substrates. In the absence of the enzyme, the O-ester would still follow this mechanism (addition−elimination through tetrahedral intermediate), whereas

(25) Ramos, M. J.; Fernandes, P. A. *Acc. Chem. Res.* **2008**, *41*, 689–698.
(26) Claeyssens, F.; Harvey, J. N.; Manby, F. R.; Mata, R. A.; Mulholland, A. J.; Ranaghan, K. E.; Schutz, M.; Thiel, S.; Thiel, W.; Werner, H. J. *Angew. Chem., Int. Ed.* **2006**, *45*, 6856–6859.
(27) Friesner, R. A.; Guallar, V. *Annu. Rev. Phys. Chem.* **2005**, *56*, 389–427.
(28) Warshel, A. *Annu. Rev. Biophys. Biol.* **2003**, *32*, 425–443.
(29) Gao, J. L.; Truhlar, D. G. *Annu. Rev. Phys. Chem.* **2002**, *53*, 467–505.
(30) Siegbahn, P. E. M.; Blomberg, M. R. A. *Chem. Rev.* **2000**, *100*, 421–437.
(31) Siegbahn, P. E. M.; Borowski, T. *Acc. Chem. Res.* **2006**, *39*, 729–738.
(32) de Visser, S. P. *J. Am. Chem. Soc.* **2006**, *128*, 9813–9824.
(33) Becke, A. D. *J. Chem. Phys.* **1993**, *98*, 5648–5652.
(34) Becke, A. D. *J. Chem. Phys.* **1993**, *98*, 1372–1377.
(35) Lee, C. T.; Yang, W. T.; Parr, R. G. *Phys. Rev. B* **1988**, *37*, 785–789.
(36) Hay, P. J.; Wadt, W. R. *J. Chem. Phys.* **1985**, *82*, 299–310.
(37) Marten, B.; Kim, K.; Cortis, C.; Friesner, R. A.; Murphy, R. B.; Ringnalda, M. N.; Sitkoff, D.; Honig, B. *J. Phys. Chem.* **1996**, *100*, 11775–11788.
(38) Tannor, D. J.; Marten, B.; Murphy, R.; Friesner, R. A.; Sitkoff, D.; Nicholls, A.; Ringnalda, M.; Goddard, W. A.; Honig, B. *J. Am. Chem. Soc.* **1994**, *116*, 11875–11882.

for the S-ester, an elimination−addition pathway would probably be viable due to the higher stability of the eliminated thiol anion.

3. Conclusion

In summary, we have described the synthesis of a thio-ester containing pro anticancer ether lipid (S-ProAEL) starting from the commercially available glycidyl ether **1**. The cytotoxic S-ProAEL was subjected to $sPLA_2$ mediated hydrolysis, and the rate of hydrolysis compared to the natural substrate was found to be slower.

To gain further insight into the mechanism for hydrolysis, molecular dynamics simulations and density functional theory calculations were carried out. The simulations did not reveal any significant differences between the two substrates and showed that S-ProAEL (S-ester) was perfectly positioned in the active site with key distances maintained when compared to the natural substrate (O-ester). In addition, water molecules could get into the active site and obtain a perfect position for hydrolysis. DFT investigations were capable of fully rationalizing the decrease of hydrolysis rate upon substitution of oxygen with sulfur as being founded in the inherent electronic differences between oxygen and sulfur.

The good correlation between experiment and theory gives further support to the use of molecular modeling to predict the activity of new substrate types prior to the actual experimental investigation. The further scope of this project is to use the valuable information obtained of the active site and the mechanism of the action of $sPLA_2$ to design and synthesize phospholipids with tunable rates of hydrolysis and thus generate liposomal drug delivery systems with different $sPLA_2$-triggered release profiles of therapeutics from liposomes at the tumor site.

Acknowledgment. G.H.P. acknowledges financial support from the Danish National Research Foundation via a grant to MEMPHYS - Center for Biomembrane Physics. Simulations were performed at the Danish Center for Scientific Computing at the University of Southern Denmark. L.L. is supported via a scholarship from the Technical University of Denmark. P.F. acknowledges financial support from the Carlsberg foundation, Lundbeck foundation and The Danish Council for Independent Research | Technology and Production Sciences.

Supporting Information Available: Detailed experimental procedures for organic synthesis of the lipids studied (including ^1H and ^{13}C NMR spectral data), preparation of liposomes, differential scanning calorimetry (DSC), activity measurements, and cytotoxicity assays; description of the computational methods applied to perform molecular dynamics simulations; mean distances and their standard deviations between selected atoms extracted from the simulations (Table S1); description of the computational method used for the DFT calculations (including Figures S1 and S2, *XYZ* coordinates, and solution-phase energies). This material is available free of charge via the Internet at http://pubs.acs.org.

JA901412J